Catch-Me-If-You-Can Infrastructure-less UWB-based Leader-Follower System for Compact UAVs

Luca Santoro, Matteo Nardello, Marco Calliari, William Cechin Guarienti,
Giordano Luchi, Daniele Fontanelli, Davide Brunelli
Department of Industrial Engineering,
University of Trento, Trento, Italy
name.surname@unitn.it

Abstract

UAVs are becoming common devices and are gradually coming into ordinary people's houses and industrial installations, while their domains of applications are continuously growing. Thanks to the development of compact and micro sized Unmanned Aerial Vehicles (UAVs), their use in dynamic and complex environments is becoming increasingly common. Many are the fields where UAVs can be exploited, from disaster rescue to logistics transportation to precision agriculture. This paper presents a Leader Follower application for Human Robot interaction. The system is based on ranging measurements and exploits only low cost UWB radio avoiding complex and expensive vision based systems. The system performance was assessed using HIL simulations and outdoor tests. The results show good accuracy and robustness of the tracking system and acceptable error levels while always ensuring the right level of safety for the human involved.

Index Terms

Ranging-based positioning, Ultra-Wide Band, Global Positioning System, Indoor positioning

I. Introduction

UAVs are becoming common devices and are gradually coming into ordinary people's houses and industrial installations, while their domains of applications are continuously growing. For instance, researchers have focused on the study of different application problems, such as autonomous navigation [1], obstacle avoidance [2], goods transportation [3], [4], logistics management [5] and precision agriculture [6].

In recent years, UAV control techniques have progressed steadily, and one of the still most investigated topics tackle the localisation and positioning problem. In the classical approach, UAVs obtain their position, and eventually the one of a target, exploiting the Global Positioning System (GPS). This approach, however, is not always reliable or available as in the case of GPS-denied environments [7], such as airports, alleys, parking lots and underground locations, where satellite signals and other technologies lack precision or fail entirely.

To solve this problem, researchers have proposed different positioning and localisation technologies. These solutions can be categorised into 3 main families: *Vision based*, like Visual-Inertial Navigation, Infrared and/or Lidar; *Radio Frequency based*, such as Ultra-Wide Band (UWB), Bluetooth and Radio Frequency IDentification; *Audio signal based*, exploiting Ultrasound technologies [8]–[11]. Among all the listed solutions, UWB presents some unique characteristics like low-cost, low latency, low energy consumption, and centimeter-level accuracy that have attracted researchers' interest lately [12], [13]. Moreover, unlike vision-based technologies, the RF will never suffer from the low-visibility condition and does not require costly infrastructures or computationally hungry processing algorithms. Therefore, fuelled by recent advancements in the development of localisation infrastructures based on UWB [14], [15], researchers have investigated the application of such technologies in robotics [16], [17], even for multi-agent formation control [18]. For instance, in [19], a combination of UWB ranging with GPS way pointing is adopted to achieve cooperative flight for cooperative goods transportation. In [20], a swarm of miniature, fully autonomous flying robots capable of exploring unknown environments autonomously while satisfying various requirements, including flight efficiency, obstacle avoidance, inter-robot collision avoidance, and swarm coordination has been presented.

As the number of personal UAVs is constantly growing, it becomes important to study the interaction between humans and such systems [21], [22]. Currently, most of the research is devoted to the evaluation and the development of new control modalities to enhance human-drone interaction and extend the set of possible use cases [23], [24]. However, the need for complex hardware interfaces, such as joysticks or haptic devices along with visual/auditory control as voice recognition or the interpretation of face poses and body postures, limits the possible use cases and the wide spread application of UAVs in service robotics scenarios [25]. In this paper, we present the preliminary results of a human-robot interaction use case in which an autonomous UAV is in charge of following a human subject exploiting only UWB-based positioning. The paradigm chosen for the UAV control is known as *Leader-Follower* and consists of an autonomous UAV follower that plans its action

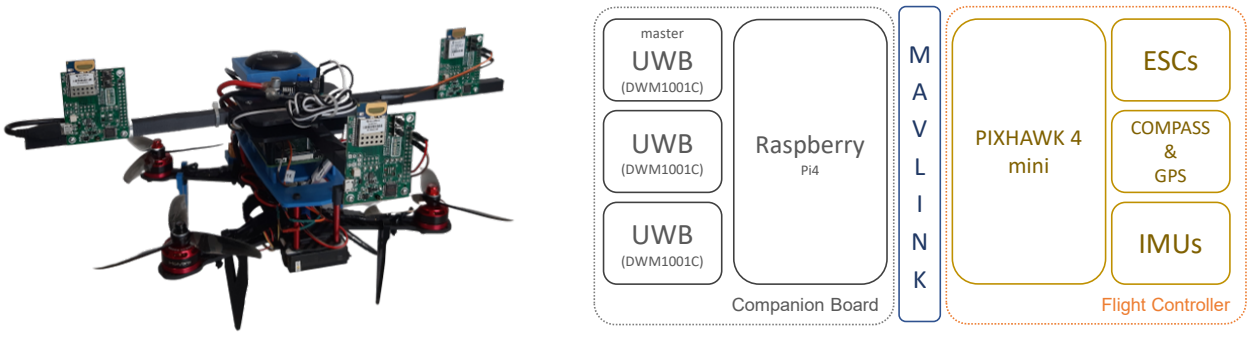

(a) (b)

Fig. 1. (a) UAV follower prototype. (b) Follower system architecture. On the left the three UWB radios along with the RPi 4 companion board. The master DWM1001C is in charge of collecting the data from the other UWB radios and stream them to the RPi 4. On the right the UAV avionics. Companion board to flight controller communication is implemented using a MAVLINK.

from the action of a human leader. This paradigm applies to different type of mobile robots and it is based on the computation of a reference point placed in the neighbours of the human being and used for scheduling its motion [26]. In the proposed application, the human being is equipped with a single UWB transceiver (referred to as the *target* or *tag*), while the follower is a compact 250 mm wheelbase UAV equipped with 3 UWB transceivers (called *anchors*) deployed in a triangular shape to avoid positioning ambiguities [27] (see Figure 1 for a snapshot of the developed UAV follower prototype). Within the described application, the main contributions of this paper are:

- An analysis of the impact of the geometric shape and baseline of the 3 UWB anchors mounted on the follower on the accuracy of the position estimates;
- The development of an algorithm that given the position estimates, track the tag with desired precision;
- The development of Hardware-in-the-Loop simulations for the algorithm evaluation and the integration of the proposed solution on a commercial compact 250 mm UAV with preliminary experimental results.

The rest of the paper is organised as follows: Section II presents the positioning algorithm and the techniques for estimating the leader location. Section III discusses the hardware in the loop simulations, UWB accuracy and presents the real outdoor test results. Section IV closes the paper with some final remarks and future outlooks.

II. The Catch-Me-If-You-Can Solution

Let us consider the UAV follower prototype reported in Figure 1, which is endowed with three UWB anchors placed at distance b with respect to the centre of mass of the UAV on an equilateral triangular configuration. The target person, i.e., the leader, is tracked using an UWB tag, whose position is determined by the Cartesian coordinates of the tag in the UAV reference frame, dubbed $\langle U \rangle$, and whose coordinates are expressed as $\mathbf{p} = [x, y, z]^T$. The three UWB anchor positions, i.e., $\mathbf{a}_i = [x_i, y_i, z_i]^T$, are known and expressed in the same reference frame $\langle U \rangle$, with $z_i = 0$, $\forall i = 1, 2, 3$, and are depicted with blue circles in Figure 2. The i-th anchor is able to deliver a distance to the UWB tag, i.e.,

$$\rho_i = \sqrt{(x_i - x)^2 + (y_i - y)^2 + (z_i - z)^2} + \eta_i = \overline{\rho}_i + \eta_i, \tag{1}$$

where η_i is the uncertainty contribution, which is supposed to be normally distributed, zero-mean and white, that is $\eta_i \sim \mathcal{N}(0, \sigma(\overline{\rho}_i)^2)$. Its variance in general depends on the actual distance $\overline{\rho}_i$ and on the UWB signal bandwidth [28]. Considering Line of Sight (LOS) conditions and neglecting shadowing and multipath effects (a customary assumption for outdoor applications), the UWB module introduces a delay in the timestamp due to internal circuitry [29], which is different for each radio and a function of the actual distance [30]. Therefore, the ranging measurements (1) turns to

$$\rho_i = \beta_i(\overline{\rho}_i) + \overline{\rho}_i + \eta_i, \tag{2}$$

where $\beta_i(\overline{\rho}_i)$ is a bias that has to be taken into account for the foreseen application.

In order to keep the structure of the UAV compact and cheap, only three planar anchors can be installed on the platform at distance b. As a consequence, having just three anchors, only planar estimates can be carried out using trilateration [31], which is, however, a quite common assumption when UAVs are considered [17]. To solve this issue for the problem at hand, we assume that the UAV collects the measurements about its height h from the ground using additional sensors (e.g., a sonar pointing downwards and/or a barometer). Assuming that the target moves on the ground as well, the z coordinate of the tag $\mathbf{p}$ in $\langle U \rangle$ along the Z_u axis (that is the axis pointing downwards in Figure 2) is actually unknown and cannot be estimated if no knowledge about the motion of the target is considered. Therefore, let us denote with d^* the desired distance between the

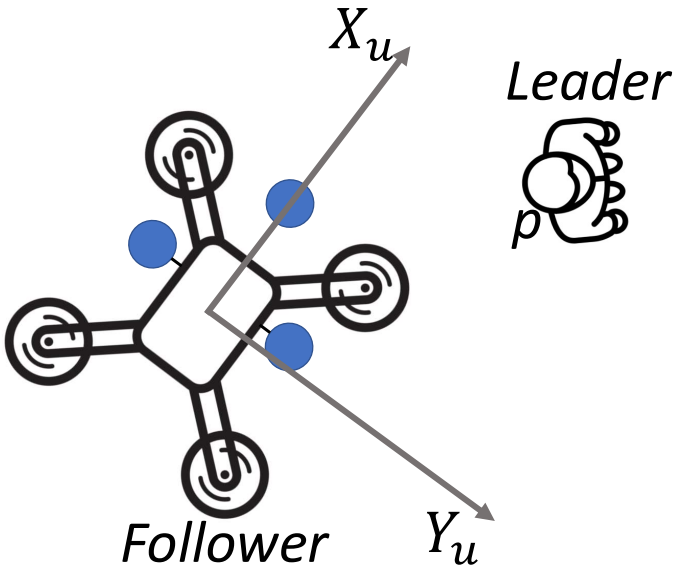

Fig. 2. Reference systems considered for the leader-follower application. The blue circles represent the positions of the three UWB anchors, all expressed in the depicted UAV reference frame $\langle U \rangle$.

leader and the follower along the X_u axis (see Figure 3), while $\overline{d}$ is the actual distance in $\langle U \rangle$, i.e., $\overline{d} = \|\mathbf{p}\| = \sqrt{x^2 + y^2 + z^2}$. If the z coordinate of the tag $\mathbf{p}$ would be known, it would be possible to consider the projection $\mathbf{p}^*$ of the vector $\mathbf{p}$ onto the $X_u \times Y_u$ plane, i.e., $\mathbf{p}^* = [x, y, 0]^T$, and then control the UAV in order to have $\mathbf{p}^* \to [d^*, 0, 0]^T$. Since the coordinate z is unknown and not observable, we conservatively assume that $z = h$, i.e., the height of the UAV from the ground, thus yielding a projection $\tilde{\mathbf{p}}^* = [x - \delta_x, y - \delta_y, 0]^T$, with $\delta_x \geq 0$ and $\delta_y \geq 0$. This way, the target appears closer than it is in reality. Hence, when $\tilde{\mathbf{p}}^* \to [d^*, 0, 0]^T$, the UAV will be at a larger distance from the leader. Notice that, in the worst scenario, that is when $z = 0$, the distance from the tag will be $\sqrt{d^{*2} + h^2}$.

Another issue to deal with is the presence of the bias, reported in (2). As a matter of fact, this bias cannot be estimated online without the knowledge of the motion of the leader. However, its effect can be highly mitigated through calibration. Indeed, by assuming that the bias is mainly induced by the available hardware, it can be considered time invariant. Albeit its value still depends on the actual distance, we can safely assume for the i-th anchor that $\beta_i(\overline{\rho}_i) \approx \beta_i(d^*)$, which allows us to increase the efficacy of this approximation once the UAV is driven towards the desired location. Similarly, we will assume that the uncertainty η_i standard deviation $\sigma(\overline{\rho}_i)$ is sufficiently small, constant and equals to σ. Therefore, we will consider from this point on the availability of the bias-compensated ranging measurement (1) instead of (2). The validity of this assumption and the calibration procedure will be investigated in Section III.

In light of the previous discussion and the conservative assumption derived, we will consider henceforth the planar problem that can be solved with a trilateration approach. In particular, we will propose two different approaches for positioning, namely the *Linear Least Square* (LLS) and the *Non-Linear Least Square* (NLLS), and the Kalman filter for continuous tracking of the leader. Notice, nonetheless, that the distance between the anchors $\mathbf{a}_i$ plays a crucial role in the reachable positioning uncertainty of the leader. Indeed, geometry matters in the deployment of the anchors for positioning problem, which can be related to the Geometric Dilution of Precision and to the Cramer-Rao Lower Bound (CRLB), as reported in [27].

A. Leader positioning solutions

In what follows, we will assume that the sampling frequency of each anchor $\mathbf{a}_i$, $i = 1, 2, 3$, is approximately the same. As reported in [32], the estimates of the planar coordinates $\mathbf{p}_r = [x, y]^T$ in $\langle U \rangle$, dubbed $\hat{\mathbf{p}}_r = [\hat{x}, \hat{y}]^T$, can be retrieved by the following unconstrained minimisation problem

$$\hat{\mathbf{p}}_r = \arg\min_{\mathbf{p}_r} \sum_{i=2}^{3} \left(\|\mathbf{p}_r - \mathbf{a}_i\|^2 - \rho_i^2 \right) - \left(\|\mathbf{p}_r - \mathbf{a}_1\|^2 - \rho_1^2 \right), \tag{3}$$

which turns to the following LLS problem and related solution

$$\hat{\mathbf{p}}_r = \arg\min_{\mathbf{p}_r} (A\mathbf{p}_r - \mathbf{c})^T (A\mathbf{p}_r - \mathbf{c}) = (A^T A)^{-1} A^T \mathbf{c} \tag{4}$$

where

$$A = -\begin{bmatrix} 2(x_2 - x_1) & 2(y_2 - y_1) \\ 2(x_3 - x_1) & 2(y_3 - y_1) \end{bmatrix},$$

and

$$\mathbf{c} = \begin{bmatrix} (x_1^2 + y_1^2 - \rho_1^2) - (x_2^2 + y_2^2 - \rho_2^2) \\ (x_1^2 + y_1^2 - \rho_1^2) - (x_3^2 + y_3^2 - \rho_3^2) \end{bmatrix},$$

and the implicit approximation that $\hat{\mathbf{p}} = [\hat{\mathbf{p}}_r^T, h]^T$, i.e., the tag is on the motion plane, as discussed above.

The NLLS solution, instead, solves the following nonlinear cost index directly

$$\hat{\mathbf{p}}_r = \arg\min_{\mathbf{p}_r} \sum_{i=1}^{3} \left(\|\mathbf{p}_r - \mathbf{a}_i\| - \rho_i \right)^2. \tag{5}$$

This problem can be solved with many different numerical methods, however it has been shown in [27] that, starting from the LLS solution (4) as first initial guess, the estimation precision reaches the CRLB with just a couple of iterations of the Gauss-Newton method.

It is worthwhile to point out that if the dynamic of the leader is slow enough in comparison with the sampling time of the anchors, it is possible to use multiple measurements from each anchor. In such a way, assuming that m_i is the number of measurements available for the i-th anchor, (3) turns to

$$\arg\min_{\mathbf{p}_r} \sum_{i=2}^{3} \sum_{j=1}^{m_i} \left(\|\mathbf{p}_r - \mathbf{a}_i\|^2 - \rho_{i,j}^2 \right) - \left(\|\mathbf{p}_r - \mathbf{a}_1\|^2 - \rho_{1,j}^2 \right),$$

while (5) turns to

$$\arg\min_{\mathbf{p}_r} \sum_{i=1}^{3} \sum_{j=1}^{m_i} \left(\|\mathbf{p}_r - \mathbf{a}_i\| - \rho_{i,j} \right)^2,$$

where $\rho_{i,j}$ stand for the j-th measurements from the anchor $\mathbf{a}_i$. Of course, in both cases, the solutions remains the same as in the single measurement case.

B. Kalman filter for tracking

The measured positions $\hat{p}_r$ obtained either by (4) or by (5) are used in the update step of a Kalman Filter (KF) that keeps track of the location of the leader in $\langle U \rangle$. Such measurements are considered affected by an uncertainty ν, which is assumed to be Gaussian, zero-mean and white, i.e., $\nu \sim \mathcal{N}(0, R)$. The covariance matrix R is hence a 2×2 matrix whose entries are experimentally determined in Section III.

Instead, for the prediction step of the KF, we first assume that both the velocity of the UAV and of the target are limited by $v_m = 2.0$ m/s, which is a standard choice when the leader is a human being walking in free space. The dynamic model considered in the prediction step represents the relative motion between the follower and the leader, i.e., a motion model expressing the difference of the dynamic between the UAV and the target. Even though human beings motion models exists in the literature, for instance [33], we decided to use a constant velocity model due to its simplicity and due to the effectiveness in non-cluttered environments [34]. The effect of such assumptions is that the motion of the human being does not change abruptly during the KF time step δ_t, which is usually the same of the sampling time of the ranging measurements and in the order of tens of milliseconds. As such, the Euclidean distance between the UAV and the tracked person does not change significantly, while a change of direction can be entirely devoted to the yaw angle rate of the UAV. Therefore, the simplified model for predicting the person's position in $\langle U \rangle$ boils down to

$$\hat{\mathbf{p}}_{f,k+1} = C_k \hat{\mathbf{p}}_{f,k} + \varepsilon_k \tag{6}$$

where $\hat{\mathbf{p}}_{f,k+1}$ is the estimate of the KF at time $(k+1)\delta_t$ and where, assuming that θ_k is the yaw of the UAV, the transition matrix

$$C_k = \begin{bmatrix} \cos(\theta_{k-1} - \theta_k) & -\sin(\theta_{k-1} - \theta_k) \\ \sin(\theta_{k-1} - \theta_k) & \cos(\theta_{k-1} - \theta_k) \end{bmatrix}.$$

The model uncertainty ε_k is responsible of the inaccurate motion model assumed, and it is generated by a Gaussian, zero-mean, white and stationary stochastic process, whose covariance matrix Q is given by

$$Q = \begin{bmatrix} (v_m \delta_t)^2 & 0 \\ 0 & (v_m \delta_t)^2 \end{bmatrix}.$$

The KF estimation error covariance matrix at time $k\delta_t$, i.e., P_k, is initialised with R, that is $P_0 = R$, since the first estimate of $\hat{\mathbf{p}}_{f,0}$ is given directly by (4) or by (5).

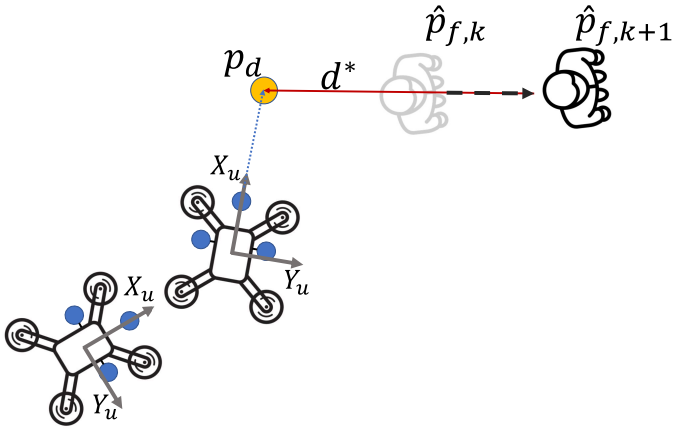

Fig. 3. Position of the UAV desired position $\mathbf{p}_d$, which is computed using two consecutive KF position estimates $\hat{\mathbf{p}}_{f,k+1}$ and $\hat{\mathbf{p}}_{f,k}$.

TABLE I
VALUE OF BIAS β_i AND σ_i FOR THE UWB ANCHORS. THE SIZE OF THE BATCH FOR EACH ANCHOR IN EACH POSITION IS OF 2000 SAMPLES.

Parameter	$\mathbf{a}_1$	$\mathbf{a}_2$	$\mathbf{a}_3$
β_i [mm]	584	695	617
σ_i [mm]	41	48	38

As reported in Figure 3, when two consecutive position estimates $\hat{\mathbf{p}}_{f,k+1}$ and $\hat{\mathbf{p}}_{f,k}$ are determined in $\langle U \rangle$ and by knowing the motion of the UAV (obtained directly by the applied control law), it is possible to identify the desired robot position $\mathbf{p}_d$, which is on the back of the leader at distance d^*. Now, the controller has all the ingredients to generate a velocity set-point $v = [v_x, v_y]^T$ for the UAV in order to move towards $\mathbf{p}_d$ and, hence, follow the target at the desired distance d^*. In particular, v is generated so as to let the UAV asymptotically approach $\mathbf{p}_d$ plus the estimated target velocity, i.e., $\frac{1}{\delta_t}(\hat{\mathbf{p}}_{f,k+1} - \hat{\mathbf{p}}_{f,k})$. To further enforce safety, the UAV stops when the detected distance to the target is smaller than d^*.

III. CHARACTERISATION AND PRELIMINARY RESULTS

A proper characterisation of the target positioning error is required for designing the system and finding the right balance among the elements to ensure the effectiveness of the system.

A. UWB characterisation and calibration

To characterise the precision and improve the accuracy of the ranging measurements, as well as to compensate for the effect of the bias term in (2), we conducted static and dynamic indoor experiments in which we compare the ranging measurements ρ_i obtained from the available UWB anchors with the distances $\overline{\rho}_i$ retrieved from the motion capture (MOCAP) system, here considered as ground truth. As aforementioned, considering an outdoor obstacle-free area, where the UWB anchors can operate in LoS conditions, we first analyse the influence of the bias $\beta_i(\overline{\rho}_i)$. From the results in Figure 4-a where the anchor $\mathbf{a}_1$ has been tested (similar results are obtained for all the other anchors), it turned out how the bias is indeed independent from $\overline{\rho}_i$, since for different actual locations of the tag, the difference between the MoCap data (blue line, corresponding to $\overline{\rho}_i$) and the UWB data (red line, corresponding to ρ_i) is approximately the same. In order to collect quantitative results, during the calibration process, we removed the outliers that consist on average of around 0.5% of each given batch of data, thus obtaining the estimates for both the bias and the standard deviations for all the anchors reported in Table I. Figure 4-(b) illustrates the histogram of the estimated distance after the bias compensation for anchor $\mathbf{a}_1$.

B. Simulation results

In this section, we assess the performance and the sensitivity of the positioning LLS and NLLS solutions presented in Section II-A through comprehensive simulations using the Gazebo simulator and with the purpose to analyse the effects of

1. Distance b between anchors and centre of mass of the UAV;
2. Bias in measurements;
3. Number of measurements available.

In the simulator the ranging measurements for the three anchors installed on the drone are corrupted by a gaussian noise $\eta \sim \mathcal{N}(0, \sigma_i^2)$ with reference to (2) and Table I.

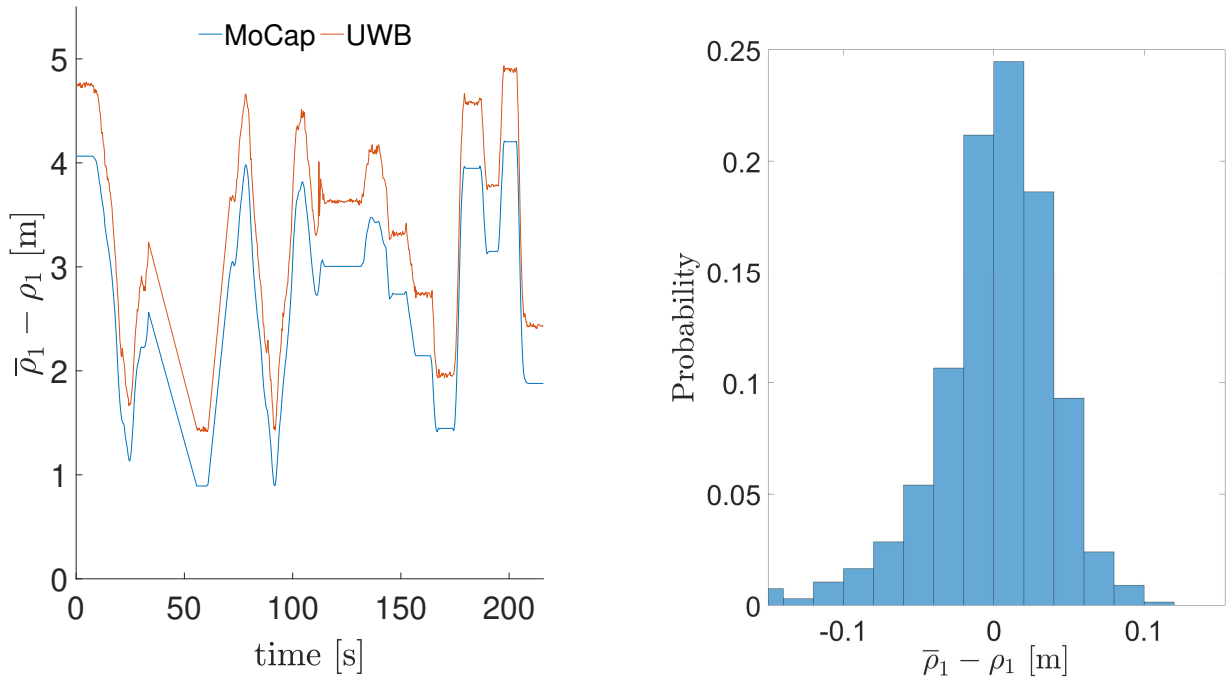

(a) (b)

Fig. 4. (a) Distance measured by $\mathbf{a}_1$ (red line) and the actual distance (blue line) to infer the bias $\beta_1(\overline{\rho}_1)$. (b) Error histogram of $\overline{\rho}_1 - \rho_1$ after the bias in Table I has been compensated.

1) Anchors distance: The three UWB anchors are deployed around the UAV centre of mass in a triangular configuration to reduce the detrimental effects of the position dilution of precision [27]. The output of this first analysis shows how the performance of the positioning method is affected by the baseline b of the anchors. To this end, we set up a Monte Carlo experiment with 52000 trials in which we vary the baseline between the anchors as $b \in [0.1, \ldots, 0.5]$ [m]. The average position error considering $m_i = 5$ repeated ranging measurements for each anchor are reported in Figure 5. As expected, the increase of the baseline b leads to a better accuracy. However, a baseline $b = 20$ cm is sufficient to have good precision and to place the radio hardware on most compact commercial drone airframes (i.e., 250-class). Moreover, we also noticed that the NLLS solution yields better results with respect to the LLS.

2) Effect of bias on measurements: WE additionally conducted Monte Carlo simulations with 4000 trials to understand the effect of the bias β_i on both the solution NLLS and LLS. In each experiment, we change the value of the bias as $\beta_i = \{0, 5, 10, 15, 20\}$ [cm]. The results obtained in the worst case are reported in Figure 6 with respect to the position error $\|\mathbf{p}_r - \hat{\mathbf{p}}_r\|$. Also in this case the error is well contained by the NLLS, while the LLS returns quite bad results. By comparing Figure 5 and Figure 6, it becomes evident how the bias calibration and compensation turns to be a clear performance booster.

3) Consistency of the position algorithms: To verify that the NLLS positioning algorithm is consistent even in our case when more data is made available [31], the following cycle is repeated N_{rep} times:

- A set of $m_i = 5$ ranging measurements between the target and each anchors is collected;
- The average position of the target is estimated using both the LLS and the NLLS algorithms.

Looking at Figure 7 we can see that increasing N_{rep} significantly improves the accuracy of the position estimate. Using the results obtained for the NLLS and with the aforementioned parameters, it is possible to compute the empirical Monte Carlo-based covariance matrix of the position estimation error for the NLLS solution to be used as the matrix R in the KF, i.e.

$$R = \mathrm{E}\left\{\mathbf{e}\mathbf{e}^T\right\} \approx \begin{bmatrix} 0.627\ \mathrm{m}^2 & 0.001\ \mathrm{m}^2 \\ 0.001\ \mathrm{m}^2 & 0.630\ \mathrm{m}^2 \end{bmatrix},$$

where $e_x = x - \hat{x}$ and $e_y = y - \hat{y}$ are the positioning errors along the X_u and Y_u axis of $\langle U \rangle$, respectively, while $\mathbf{e} = [e_x - \mathrm{E}\{e_x\}, e_y - \mathrm{E}\{e_y\}]^T$.

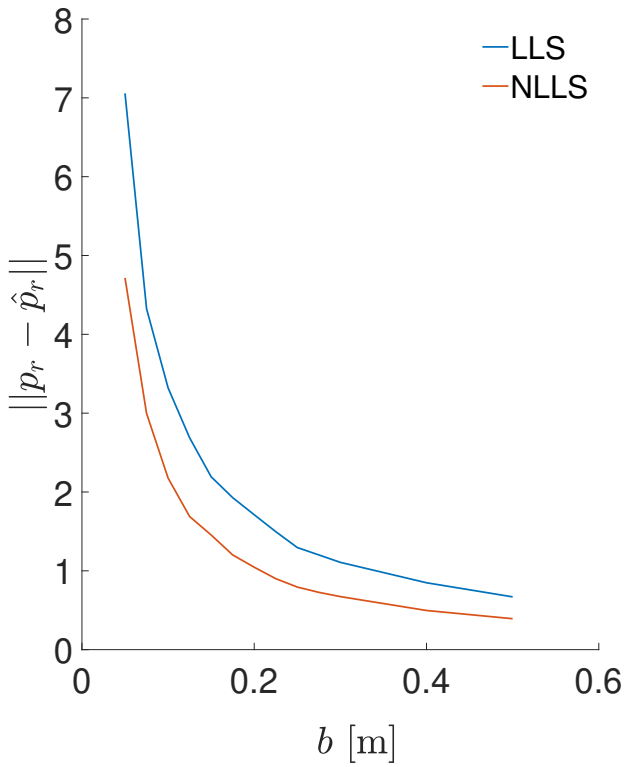

Fig. 5. Average position error $\|\mathbf{p}_r - \hat{\mathbf{p}}_r\|$ of the Monte Carlo simulations for different values of the baseline b and for both the LLS and the NLSS solutions.

C. Validation

A Hardware-in-the-Loop (HITL) experiment was conducted to validate the proposed low-cost UWB-based person tracking system. Based on the previous analysis, the distance between the UAV centre and the UWB anchors is chosen to be $b = 20$ cm, while the number of repeated measurements for each UWB radio is set to $m_i = 5$. To test the positioning and control algorithms, a typical motion pattern is applied to the target based on [35], as shown in Figure 8.

The histogram of the error of the estimated positions is shown in Figure 9. It can be noticed that, despite the approximations described, the error remains limited even in the human beings sharp change of directions reported in Figure 8-b.

D. Preliminary experimental results

At the stage of the writing, the outdoor test are executed without a ground truth. In Figure 10 is shown a frame of the outdoor test, while a full video of the experiment is available at the following link[1]. In the video material, there is a manoeuvre, called *twirl*, executed during the lock on target: its purpose is only to give a visual feedback to the user and increase the user confidence and trustfulness. The outdoor experiments are very promising and the system was able to correctly track the human being at the desired distance with minor errors (in the order of some tens of centimetres) even along sharp turns.

IV. Conclusion

In this paper, we have proposed a solution for unmanned aerial vehicle target tracking based on onboard UWB ranging measurements. The main focus of this work has been the design of all the hardware and software architecture required to accomplish the goal mentioned above. After briefly describing the UWB transceiver, we characterised its measurement process and presented the NLLS and LLS algorithms, which solve the trilateration problem and retrieve a position estimate. A Monte Carlo analysis has been performed to validate the two methods and to set some design parameters. In order to avoid sharp variations of the point to track, a Kalman filter-based tracking system has been developed as well. Hardware in the loop simulations and preliminary experimental results showed a very smooth behaviour of the UAV under acceptable accuracy performance given the considered simple and cheap design choices.

[1]https://www.youtube.com/watch?v=_SPHzfz6aXU

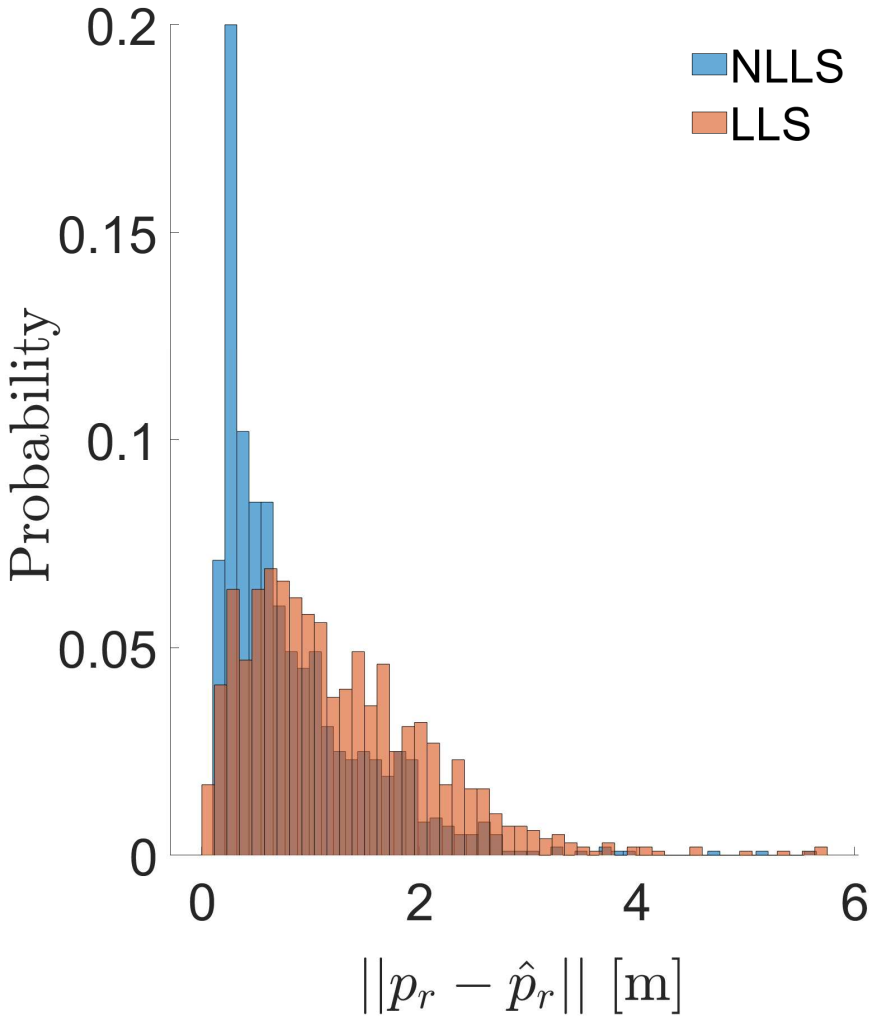

Fig. 6. Histogram of the position error $\|\mathbf{p}_r - \hat{\mathbf{p}}_r\|$ for the NLLS and LLS solutions with a bias $\beta_i = 0.2$ m.

For future works, we firstly aim at testing the system in a more challenging outdoor scenario and using external MoCap systems for ground truth generation. Then, we aim at improving the proposed solution with more advanced estimation filters endowed with more sophisticated human motion models as well as at implementing tailored control policy. Finally, we are currently studying the possibility to estimate the height of the tag when the human is standing still and the UAV undergoes specifically conceived controlled manoeuvres.

REFERENCES

[1] T. Elmokadem and A. V. Savkin, "Towards fully autonomous uavs: A survey," *Sensors*, vol. 21, no. 18, 2021. [Online]. Available: https://www.mdpi.com/1424-8220/21/18/6223

[2] J. Tang, S. Lao, and Y. Wan, "Systematic review of collision-avoidance approaches for unmanned aerial vehicles," *IEEE Systems Journal*, pp. 1–12, 2021.

[3] A. Gupta, T. Afrin, E. Scully, and N. Yodo, "Advances of uavs toward future transportation: The state-of-the-art, challenges, and opportunities," *Future Transportation*, vol. 1, no. 2, pp. 326–350, 2021. [Online]. Available: https://www.mdpi.com/2673-7590/1/2/19

[4] I. Khoufi, A. Laouiti, and C. Adjih, "A survey of recent extended variants of the traveling salesman and vehicle routing problems for unmanned aerial vehicles," *Drones*, vol. 3, no. 3, 2019. [Online]. Available: https://www.mdpi.com/2504-446X/3/3/66

[5] M. Kloetzer, A. Burlacu, G. Enescu, S. Caraiman, and C. Mahulea, "Optimal indoor goods delivery using drones," in *2019 24th IEEE International Conference on Emerging Technologies and Factory Automation (ETFA)*, 2019, pp. 1579–1582.

[6] N. Delavarpour, C. Koparan, J. Nowatzki, S. Bajwa, and X. Sun, "A technical study on uav characteristics for precision agriculture applications and associated practical challenges," *Remote Sensing*, vol. 13, no. 6, 2021. [Online]. Available: https://www.mdpi.com/2072-4292/13/6/1204

[7] B. Yang and E. Yang, "A survey on radio frequency based precise localisation technology for uav in gps-denied environment," *Journal of Intelligent & Robotic Systems*, vol. 103, no. 3, p. 38, Oct 2021. [Online]. Available: https://doi.org/10.1007/s10846-021-01500-4

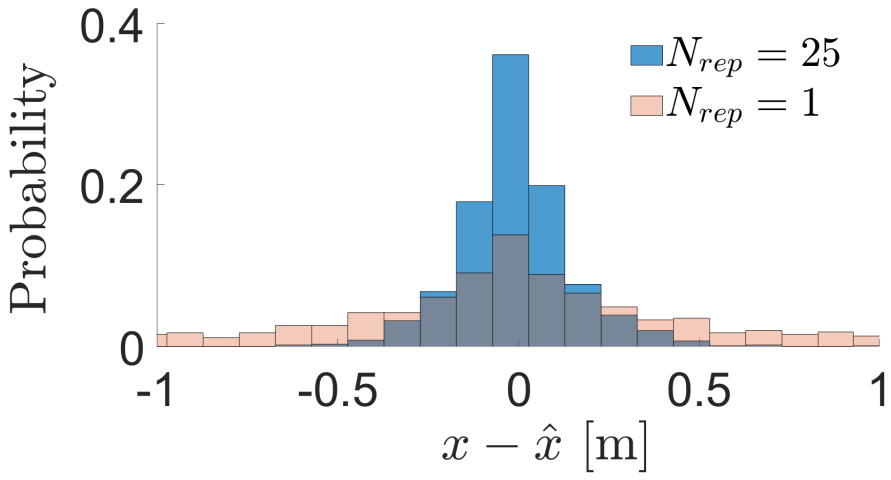

(a)

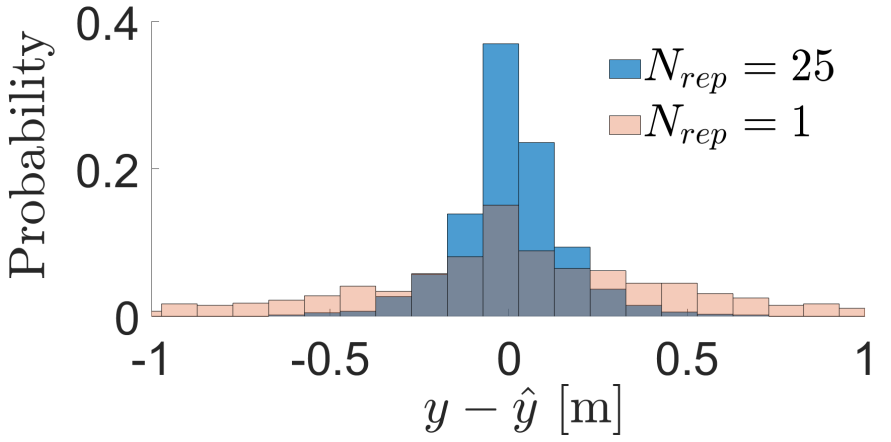

(b)

Fig. 7. Distributions of error $e_x = x - \hat{x}$ and $e_y = y - \hat{y}$ for the solutions with $N_{rep} = \{1, 25\}$.

[8] G. Huang, "Visual-inertial navigation: A concise review," in *2019 International Conference on Robotics and Automation (ICRA)*, 2019, pp. 9572–9582.

[9] N. Gyagenda, J. V. Hatilima, H. Roth, and V. Zhmud, "A review of gnss-independent uav navigation techniques," *Robotics and Autonomous Systems*, vol. 152, p. 104069, 2022. [Online]. Available: https://www.sciencedirect.com/science/article/pii/S0921889022000343

[10] G. Balamurugan, J. Valarmathi, and V. P. S. Naidu, "Survey on uav navigation in gps denied environments," in *2016 International Conference on Signal Processing, Communication, Power and Embedded System (SCOPES)*, 2016, pp. 198–204.

[11] R. Kapoor, S. Ramasamy, A. Gardi, and R. Sabatini, "Uav navigation using signals of opportunity in urban environments: A review," *Energy Procedia*, vol. 110, pp. 377–383, 2017, 1st International Conference on Energy and Power, ICEP2016, 14-16 December 2016, RMIT University, Melbourne, Australia. [Online]. Available: https://www.sciencedirect.com/science/article/pii/S1876610217301868

[12] Z. Silvia, C. Martina, S. Fabio, and P. Alessandro, "Ultra wide band indoor positioning system: analysis and testing of an ips technology," *IFAC-PapersOnLine*, vol. 51, no. 11, pp. 1488–1492, 2018, 16th IFAC Symposium on Information Control Problems in Manufacturing INCOM 2018. [Online]. Available: https://www.sciencedirect.com/science/article/pii/S2405896318314162

[13] A. Alarifi, A. Al-Salman, M. Alsaleh, A. Alnafessah, S. Al-Hadhrami, M. A. Al-Ammar, and H. S. Al-Khalifa, "Ultra wideband indoor positioning technologies: Analysis and recent advances," *Sensors*, vol. 16, no. 5, 2016. [Online]. Available: https://www.mdpi.com/1424-8220/16/5/707

[14] L. Santoro, M. Nardello, D. Brunelli, and D. Fontanelli, "Scale up to infinity: the uwb indoor global positioning system," in *2021 IEEE International Symposium on Robotic and Sensors Environments (ROSE)*, 2021, pp. 1–8.

[15] B. Yang, E. Yang, L. Yu, and A. Loeliger, "High-precision uwb-based localisation for uav in extremely confined environments," *IEEE Sensors Journal*, vol. 22, no. 1, pp. 1020–1029, 2022.

[16] V. Magnago, P. Corbalán, G. Picco, L. Palopoli, and D. Fontanelli, "Robot Localization via Odometry-assisted Ultra-wideband Ranging with Stochastic Guarantees," in *Proc. IEEE/RSJ International Conference on Intelligent Robots and System (IROS)*. Macao, China: IEEE, Nov. 2019, pp. 1607–1613.

[17] L. Santoro, D. Brunelli, and D. Fontanelli, "On-line Optimal Ranging Sensor Deployment for Robotic Exploration," *IEEE Sensors Journal*, vol. 22, no. 6, March 2022.

[18] S. Lee, C. Park, S.-Y. Lee, J. H. Jeon, and D. Lee, "Uwb based relative navigation and leader-follower formation for uavs using maneuvering of a follower," in *2021 21st International Conference on Control, Automation and Systems (ICCAS)*, 2021, pp. 239–243.

[19] T. Chen, Q. Gao, and M. Guo, "An improved multiple uavs cooperative flight algorithm based on leader follower strategy," in *2018 Chinese Control And Decision Conference (CCDC)*, 2018, pp. 165–169.

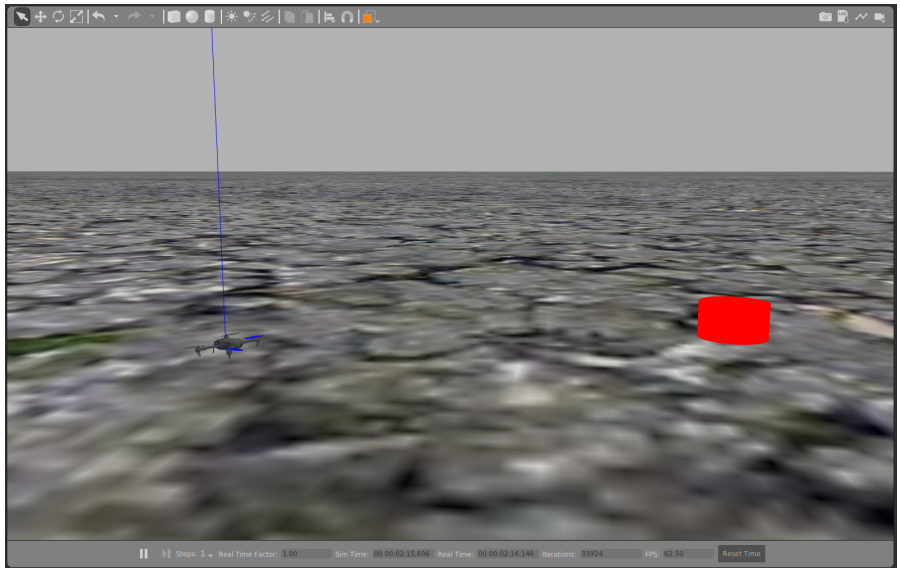

(a)

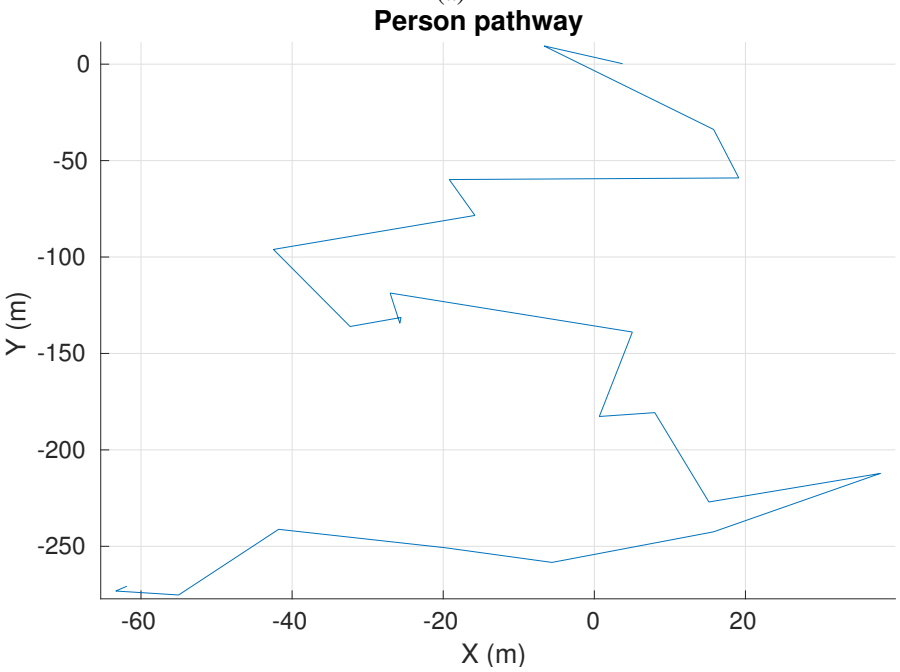

(b)

Fig. 8. (a) Gazebo simulation environment with the UAV (a quadrotor) and the target (represented by the red cylinder). (b) The path traveled by the target.

[20] X. Zhou, X. Wen, Z. Wang, Y. Gao, H. Li, Q. Wang, T. Yang, H. Lu, Y. Cao, C. Xu, and F. Gao, "Swarm of micro flying robots in the wild," *Science Robotics*, vol. 7, no. 66, p. eabm5954, 2022. [Online]. Available: https://www.science.org/doi/abs/10.1126/scirobotics.abm5954

[21] M. Obaid, W. Johal, and O. Mubin, "Domestic drones: Context of use in research literature," in *Proceedings of the 8th International Conference on Human-Agent Interaction*, ser. HAI '20. New York, NY, USA: Association for Computing Machinery, 2020, p. 196–203. [Online]. Available: https://doi.org/10.1145/3406499.3415076

[22] J. R. Cauchard, J. L. E, K. Y. Zhai, and J. A. Landay, "Drone and me: an exploration into natural human-drone interaction," in *Proceedings of the 2015 ACM international joint conference on pervasive and ubiquitous computing*, 2015, pp. 361–365.

[23] S. Rajappa, H. Bülthoff, and P. Stegagno, "Design and implementation of a novel architecture for physical human-uav interaction," *The International Journal of Robotics Research*, vol. 36, no. 5-7, pp. 800–819, 2017. [Online]. Available: https://doi.org/10.1177/0278364917708038

[24] D. Tezza and M. Andujar, "The state-of-the-art of human–drone interaction: A survey," *IEEE Access*, vol. 7, pp. 167 438–167 454, 2019.

[25] K. D. Karjalainen, A. E. S. Romell, P. Ratsamee, A. E. Yantac, M. Fjeld, and M. Obaid, "Social drone companion for the home environment: A user-centric exploration," ser. HAI '17. New York, NY, USA: Association for Computing Machinery, 2017, p. 89–96. [Online]. Available: https://doi.org/10.1145/3125739.3125774

[26] R. Rafifandi, D. L. Asri, E. Ekawati, and E. M. Budi, "Leader–follower formation control of two quadrotor uavs," *SN Applied Sciences*, vol. 1, no. 6, p. 539, May 2019. [Online]. Available: https://doi.org/10.1007/s42452-019-0551-z

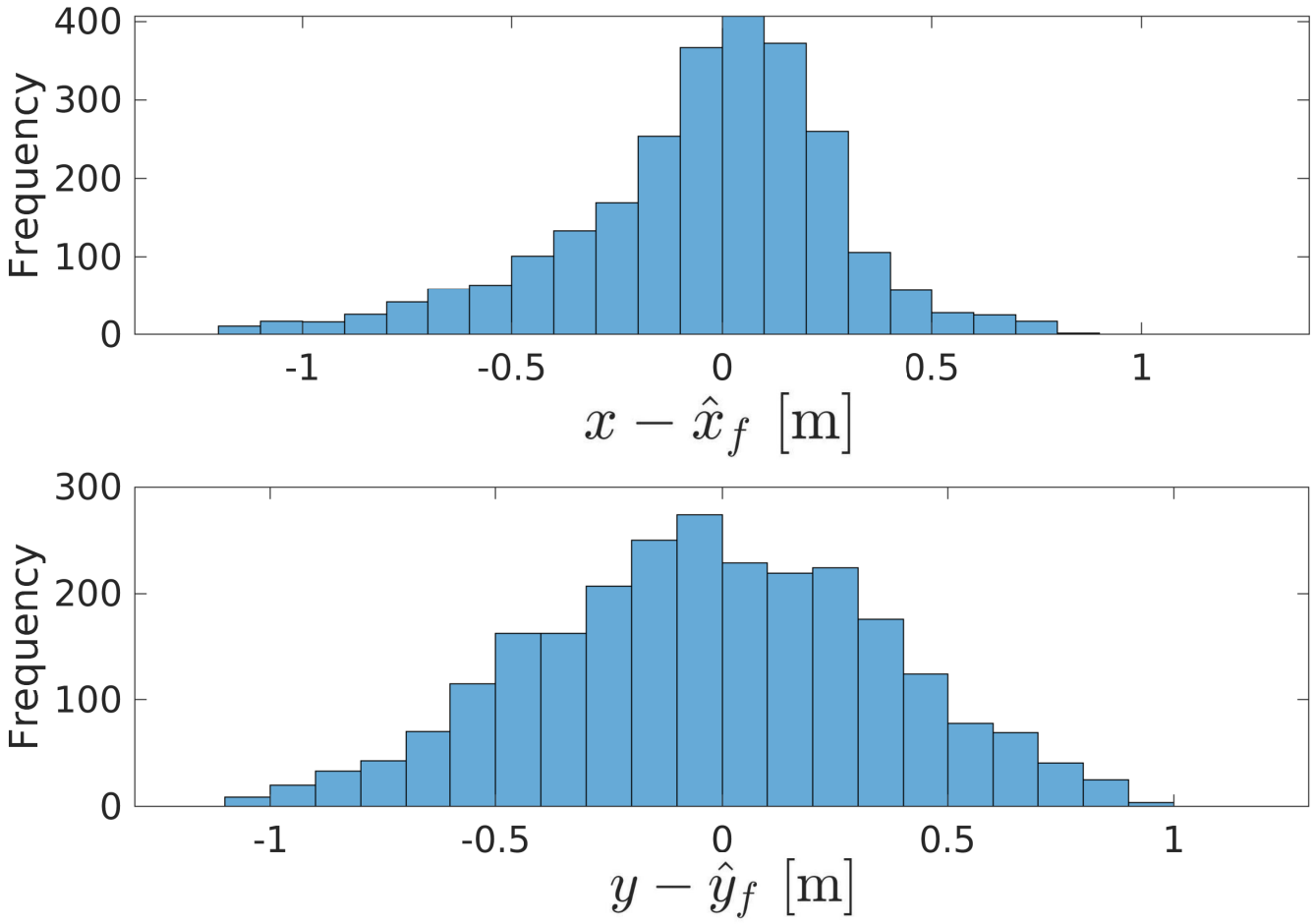

Fig. 9. Histogram of the tracking error $x - \hat{x}_f$ and $y - \hat{y}_f$ returned by the KF.

[27] D. Fontanelli, F. Shamsfakhr, and L. Palopoli, "Cramer-Rao Lower Bound Attainment in Range-only Positioning using Geometry: The G-WLS," *IEEE Trans. on Instrumentation and Measurement*, vol. 70, pp. 1–14, October 2021.

[28] J. Yan, "Algorithms for indoor positioning systems using ultra-wideband signals," 2010.

[29] A. De Preter, G. Goysens, J. Anthonis, J. Swevers, and G. Pipeleers, "Range bias modeling and autocalibration of an uwb positioning system," in *2019 International Conference on Indoor Positioning and Indoor Navigation (IPIN)*. IEEE, 2019, pp. 1–8.

[30] V. Di Pietra, P. Dabove, M. Piras, and A. Lingua, "Evaluation of positioning and ranging errors for uwb indoor applications." in *IPIN (Short Papers/Work-in-Progress Papers)*, 2019, pp. 227–234.

[31] R. Zekavat and R. M. Buehrer, *Handbook of position location: Theory, practice and advances*. John Wiley & Sons, 2011, vol. 27.

[32] D. Fontanelli, F. Shamsfakhr, D. Macii, and L. Palopoli, "An Uncertainty-driven and Observability-based State Estimator for Nonholonomic Robots," *IEEE Trans. on Instrumentation and Measurement*, vol. 70, pp. 1–12, January 2021.

[33] F. Farina, D. Fontanelli, A. Garulli, A. Giannitrapani, and D. Prattichizzo, "Walking Ahead: The Headed Social Force Model," *PLOS ONE*, vol. 12, no. 1, pp. 1–23, 1 2017.

[34] A. Antonucci, G. R. Papini, P. Bevilacqua, L. Palopoli, and D. Fontanelli, "Efficient Prediction of Human Motion for Real-Time Robotics Applications with Physics-inspired Neural Networks," *IEEE Access*, vol. 10, pp. 144–157, December 2021.

[35] H. Hicheur, S. Vieilledent, M. J. Richardson, T. Flash, and A. Berthoz, "Velocity and curvature in human locomotion along complex curved paths: a comparison with hand movements," *Experimental brain research*, vol. 162, no. 2, pp. 145–154, 2005.

Fig. 10. Preliminary outdoor test.